

MCCS: a novel recognition pattern-based method for fast track discovery of anti-SARS-CoV-2 drugs

Zhiwei Feng[†], Maozi Chen[†], Ying Xue, Tianjian Liang, Hui Chen, Yuehan Zhou, Thomas D. Nolin, Randall B. Smith and Xiang-Qun Xie

Corresponding authors: Zhiwei Feng, School of Pharmacy, University of Pittsburgh, Pittsburgh, PA 15261, USA. Tel: 412-419-4896; Fax: 412-383-7436; E-mail: zh11@pitt.edu; Xiang-Qun Xie, School of Pharmacy, University of Pittsburgh, Pittsburgh, PA 15261, USA. Tel: 412-383-5276; Fax: 412-383-7436; E-mail: xix15@pitt.edu

[†]The authors wish it to be known that, in their opinion, the first two authors should be regarded as joint first authors.

Abstract

Given the scale and rapid spread of the coronavirus disease 2019 (COVID-19) caused by severe acute respiratory syndrome coronavirus 2 (SARS-CoV-2, or 2019-nCoV), there is an urgent need to identify therapeutics that are effective against COVID-19 before vaccines are available. Since the current rate of SARS-CoV-2 knowledge acquisition via traditional research methods is not sufficient to match the rapid spread of the virus, novel strategies of drug discovery for SARS-CoV-2 infection are required. Structure-based virtual screening for example relies primarily on docking scores and does not take the importance of key residues into consideration, which may lead to a significantly higher incidence rate of false-positive results. Our novel *in silico* approach, which overcomes these limitations, can be utilized to quickly evaluate FDA-approved drugs for repurposing and combination, as well as designing new chemical agents with therapeutic potential for COVID-19. As a result, anti-HIV or antiviral drugs (lopinavir, tenofovir disoproxil, fosamprenavir and ganciclovir), antinfluenza drugs (peramivir and zanamivir) and an anti-HCV drug (sofosbuvir) are predicted to bind to 3CL^{Pro} in SARS-CoV-2 with therapeutic

Zhiwei Feng is currently an assistant professor in the School of Pharmacy, University of Pittsburgh. His research interests include (i) the development of algorithms/tools/apps for drug discovery, (ii) chemogenomic knowledgebase design and novel tool development for drug design of small molecules and modulators and (iii) big-data or clinical data analysis and pharmacometrics and systems pharmacology.

Maozi Chen is currently conducting research work in the School of Pharmacy, University of Pittsburgh. His research interests are algorithm design and software development.

Ying Xue is currently an assistant professor in the School of Pharmacy, University of Pittsburgh. Her research interests include clinical pharmacy, outcomes research and systems pharmacology.

Tianjian Liang is currently a second year's master student in the School of Pharmacy, University of Pittsburgh. His research interests are antibody drug design and systems pharmacology analysis.

Hui Chen is currently a P3 PharmD student in the School of Pharmacy, University of Pittsburgh. Her research mainly focuses on the computer-aided vaccine design.

Yuehan Zhou is currently a P2 PharmD student in the School of Pharmacy, University of Pittsburgh. His research mainly focuses on the computer-aided drug discovery of COVID-19.

Thomas D. Nolin is currently an associate professor in the School of Pharmacy, University of Pittsburgh. His research focuses on developing an understanding of the impact of kidney disease and renal replacement therapy (RRT) on nonrenal metabolism and transport pathways and corresponding effects on drug exposure and response.

Randall B. Smith is a professor and Senior Associate Dean at the University of Pittsburgh School of Pharmacy. He has extensive experience in research and the management of research for drug development and demonstration of the value of pharmaceutical products. Smith's current research interests are in the development and application of novel systems of health care delivery and education of health professionals.

Xiang-Qun Xie received his PhD degree in 1993 from the University of Connecticut. He is an Associate Dean of the School of Pharmacy, a professor of Pharmaceutical Sciences and Director/PI of NIH Center of Excellence for Computational Drug Abuse Research and Computational Chemogenomics Screening Center at the University of Pittsburgh. He serves as a Charter Member of the US FDA Science Advisory Board. He is Director of Pharmacometrics & System Pharmacology (PSP) Graduate Program for preclinical and clinical education & research. Xie is known for his pioneering research for the development of renowned 'Big-Data to Knowledge' diseases-specific chemogenomics knowledgebases platform implemented with GPU-accelerated machine-/deep-learning computational TargetHunter system pharmacology for translational medicinal chem-biology drug discovery.

Submitted: 7 July 2020; Received (in revised form): 17 August 2020

potential for COVID-19 infection by our new protocol. In addition, we also propose three antidiabetic drugs (acarbose, glyburide and tolazamide) for the potential treatment of COVID-19. Finally, we apply our new virus chemogenomics knowledgebase platform with the integrated machine-learning computing algorithms to identify the potential drug combinations (e.g. remdesivir+chloroquine), which are congruent with ongoing clinical trials. In addition, another 10 compounds from CAS COVID-19 antiviral candidate compounds dataset are also suggested by Molecular Complex Characterizing System with potential treatment for COVID-19. Our work provides a novel strategy for the repurposing and combinations of drugs in the market and for prediction of chemical candidates with anti-COVID-19 potential.

Key words: MCCS; COVID-19; residue energy contribution; drug repurposing; drug combination

Introduction

The outbreak of the coronavirus disease 2019 (COVID-19), caused by severe acute respiratory syndrome coronavirus 2 (SARS-CoV-2) [1–6], quickly spread over 213 countries/regions, infecting >21 930 883 individuals globally with more than 774 997 deaths worldwide as reported of 17 August 2020. New and effective anti-COVID-19 drugs are urgently needed, whereas a new drug discovery takes >8 years and costs >\$2.6 billion with an approval rate of less than 12% [7]. A few medications including lopinavir-ritonavir, remdesivir and hydroxychloroquine/chloroquine have been used in clinics, but there are still not enough medical data confirming these drugs work and are safe to cure COVID-19. Although lopinavir/ritonavir shows benefit in some secondary endpoints, no benefit is observed with treatment beyond standard care for severe COVID-19 patients [8], and future trials will be carried out to verify this result. Moreover, a report from France's drug safety agency disclosed that hydroxychloroquine can have serious cardiovascular side effects [9]. Gilead Sciences tracked the responses to remdesivir intervention therapy for 53 patients with COVID-19 and observed a 13% death rate [10]. However, study groups were spread out across several countries with small numbers of patients, and it is hard to draw definitive conclusions from these data. Since most of the drugs or drug combinations currently used in clinical trials are chosen empirically, there is a critical need to leverage innovative technology with available medical resources to rapidly repurpose FDA-approved drugs and select drug combinations for anti-COVID-19 before vaccines are available.

SARS-CoV-2, Middle East Respiratory Syndrome Coronavirus (MERS-CoV) and Severe Acute Respiratory Syndrome Coronavirus (SARS-CoV) are members of the coronavirus (CoV) family [11]. These CoVs can all transmit from human-to-human [12–14]. CoV infection can be as mild as the common cold or as deadly as the SARS infection. Based on the confirmed cases, the symptoms of SARS-CoV-2 include fever, malaise, dry cough, shortness of breath, respiratory distress and more. Although there are no approved medications or vaccines for COVID-19, new information regarding SARS-CoV-2 is being revealed daily. Recently, the SARS-CoV-2 has been sequenced and several important proteins have been resolved [15–19], thereby facilitating exploration and discovery of effective treatments. The rationale for repurposing and discovery of drugs for treatment of SARS-CoV-2 is based on the premise that: (i) the entry of SARS-CoV-2 into human host cells relies on the binding of spike protein (S-protein) [19] to the angiotensin-converting enzyme 2 (ACE2) [17, 20], and (ii) the replication of nCoV requires the viral 3C-like cysteine protease (3CL^{Pro}) [18] or RNA-dependent RNA polymerase (RdRp) [15], with both 3CL^{Pro} and RdRp highly conserved within the coronavirus family. These

proteins and/or enzymes are potential targets since they are involved in the mechanism of COVID-19 infection, and drugs or chemical agents targeting them may provide therapeutic potential for the treatment of COVID-19.

In recent years, computational techniques have become more common in drug design because of advantages such as time-saving, high efficiency and high sensitivity. Many *in silico* tools or approaches have been used to design and discover the potential drug candidates for COVID-19. For example, Jin et al. [18] recently resolved the 3D complex of 3CL^{Pro}-N3. Based on this crystal structure, they applied Glide algorithm to carry out a virtual screening against their in-house database and identified cinanserin (IC₅₀: 125 μ M) as a potential inhibitor for 3CL^{Pro} of SARS-CoV-2 [18]. Similarly, Wang [21] applied virtual docking screening using Glide and molecular dynamics simulation with MM-GBSA to predict the potential drug candidates for 3CL^{Pro}. Recently, Liu et al. [22] developed and applied their computational protocol SCAR (steric-classes alleviating receptors) to discover potential covalent drugs for SARS-CoV-2. In addition, several computational tools or databases have been developed to meet the urgent need of drug discovery for COVID-19, including a network-based approach for drug repurposing [23], MolAIcal [24] (a *de novo* approach, <https://molaical.github.io/quickstart.html>), COVID-19 Docking Server (<https://ncov.schanglab.org.cn/>) [25] and more. Among these methods, structure-based virtual docking screening is a popular approach for the drug discovery of COVID-19. However, structure-based virtual docking screening relies primarily on docking scores and does not take the contributions of key residues into consideration of selecting the binding pose, which may lead to a significantly higher incidence rate of false-positive results.

We have elaborated on a scoring function-based computing protocol Molecular Complex Characterizing System (MCCS) [26] to aid in rational drug design. Briefly, MCCS first calculates the energy contribution of each residue involved in the binding, which helps in determining the key residues and their energy contributions. Then, a (protein) sequence-based vector embedded with individual residue energy contribution is constructed to represent the recognition pattern or feature between a receptor and its ligand. MCCS takes the contribution and importance of key residue into consideration for selecting a more accurate binding pose during the process. Finally, the reliable energy contribution vectors are used to select potential candidates, which may improve the accuracy of virtual screening.

In the present work, we first determine the residue energy contributions in the binding pocket of 3CL^{Pro}, the main viral protease required for SARS-CoV or SARS-CoV-2 replication, toward binding an inhibitor by applying our recently developed MCCS [26] to the 3CL^{Pro}-inhibitor co-crystal structure. Then, several

3CL^{Pro}-ligand complexes are used to create energy contribution vector(s) to characterize the recognition pattern of 3CL^{Pro} in SARS-CoV/SARS-CoV-2 and virtual screening is carried out subsequently against the DrugBank database and the CAS COVID-19 antiviral candidate compounds dataset. Anti-HIV/antiviral drugs (lopinavir, tenofovir disoproxil, fosamprenavir and ganciclovir), anti-flu drugs (peramivir and zanamivir) and an anti-HCV drug (sofosbuvir) are predicted to bind to 3CL^{Pro} in SARS-CoV-2 with therapeutic potential for COVID-19 infection. Moreover, 10 additional antiviral chemicals from the CAS dataset are also predicted as promising agents for COVID-19. Finally, we also utilize our novel virus chemogenomics knowledgebase platform [27] to identify potential combinations of medications for COVID-19.

Materials and Methods

Scoring function

The scoring function in nature is not limited to the conformational search and optimization process in docking, but also it is mainly used to evaluate an entire protein-ligand complex, or more specifically, a ligand conformation inside a receptor binding site. By revisiting the atom level and aggregating the energy per residue instead of per protein, we serve the distinguishing characteristics of each residue in the process of protein-ligand binding, which also further enables the feature modeling of a protein in terms of binding.

Below are the five core terms used by the scoring function in Vina [28] and idock [29]:

$$\text{gauss}_1(d_{ij}) = e^{-\left(\frac{d_{ij}}{0.5}\right)^2}$$

$$\text{gauss}_2(d_{ij}) = e^{-\left(\frac{d_{ij}-3}{2}\right)^2}$$

$$\text{repulsion}(d_{ij}) = \begin{cases} d_{ij}^2, & \text{if } d_{ij} < 0 \\ 0, & \text{if } d_{ij} \geq 0 \end{cases}$$

$$\text{hydrophobic}(d_{ij}) = \begin{cases} 1, & \text{if hydrophobic and } d_{ij} \leq 0.5 \\ 1.5 - d_{ij}, & \text{if hydrophobic and } 0.5 < d_{ij} < 1.5 \\ 0, & \text{if not hydrophobic or } d_{ij} \geq 1.5 \end{cases}$$

$$\text{hbonding}(d_{ij}) = \begin{cases} 1, & \text{if hbonding and } d_{ij} \leq -0.7 \\ \frac{d_{ij}}{-0.7}, & \text{if hbonding and } -0.7 < d_{ij} < 0 \\ 0, & \text{if not hbonding or } d_{ij} \geq 0 \end{cases}$$

In a typical docking process, a computed atom pair consists of one atom from the protein and the other from the small molecule. Essentially the energy terms are related to three variables: the distance between, and the van der Waals radii of the two interacting atoms. By introducing a new variable d_{ij} to represent the surface distance between the interacting atoms, the functions can be reduced to unary functions of d_{ij} . In this model, atom interactions are divided into three kinds: regular interaction, hydrophobic interaction or hydrogen bond interaction. The $\text{hydrophobic}(d_{ij})$ and the $\text{hbonding}(d_{ij})$ functions evaluate to a nonzero value only if the atom pair is of the hydrophobic interaction or the hydrogen bond, respectively.

The weighted sum of the five terms forms the total score, where the coefficients are also given in the original Vina literature:

$$\begin{aligned} \text{score_atom}(d_{ij}) = & (-0.035579) * \text{gauss}_1(d_{ij}) \\ & + (-0.005156) * \text{gauss}_2(d_{ij}) \\ & + (+0.840245) * \text{repulsion}(d_{ij}) \\ & + (-0.035069) * \text{hydrophobic}(d_{ij}) \\ & + (-0.587439) * \text{hbonding}(d_{ij}) \end{aligned}$$

The residue energy contribution is calculated as

$$\text{score_residue} = \sum_{\substack{i \in R \\ j \in L}} \text{score_atom}(d_{ij})$$

where R is the set of atoms in the residue being considered, and L is the set of atoms in the ligand whose coordinates are either computed from Monte Carlo based docking or determined by X-ray crystallography or cryo-EM. Since the hydrophobic and hydrogen bond interactions are both one term more than a regular interaction, the additional terms are the key to making a residue prominent.

Similarity and clustering

To quantify the similarity between two vectors, a real-valued similarity function is used in statistics and related fields. Such similarity measures include cosine similarity, the Pearson correlation coefficient (the PCC), Euclidean distance, etc. Among all the various similarity measures, cosine similarity and the PCC are commonly used for real-valued vectors, which are suitable in our scenario.

Given two vectors of residue energy contribution, \mathbf{u} and \mathbf{v} , the cosine similarity, $\cos(\theta)$, is represented using a dot product and vector length as

$$\cos(\theta) = \frac{\mathbf{u} \cdot \mathbf{v}}{\|\mathbf{u}\| \|\mathbf{v}\|} = \frac{\sum_{i=1}^n u_i v_i}{\sqrt{\sum_{i=1}^n u_i^2} \sqrt{\sum_{i=1}^n v_i^2}}$$

where θ is the angle between the two vectors and the subscript i refers to the residue numbering under the selected scheme. The function gives a positive value (up to one) for similar vectors and either zero or a negative value for distinct vectors.

The PCC is defined in the same way except it subtracts the mean from every vector element:

$$\rho(\mathbf{u}, \mathbf{v}) = \frac{\text{cov}(\mathbf{u}, \mathbf{v})}{\sigma_u \sigma_v} = \frac{\sum_{i=1}^n (u_i - \bar{u})(v_i - \bar{v})}{\sqrt{\sum_{i=1}^n (u_i - \bar{u})^2} \sqrt{\sum_{i=1}^n (v_i - \bar{v})^2}}$$

With any similarity measure, protein clustering can be carried out in such a way that proteins in the same group are more alike, in terms of binding mode, to each other than to that of other groups. In the visualization, a heatmap of an (n, n) -sized similarity matrix is commonly used to show similarities among a set of n vectors, with a dendrogram for demonstration of the clustering. The grids of the heatmap use a color scale to display a color mapped from its numeric value which represents the similarity between two vectors. The clustering can be carried out directly with the n vectors or with the similarity rows or columns of the n vectors.

Table 1. Top 10 residue energy contributions in the complex of 3CL^{Pro} with SID-24808289 (PDB: 4MDS) (kcal/mol)

Residue	Total energy contribution	Sum of steric components ^a	Sum of hydrophobic components ^b	Sum of hydrogen-bonding components ^c
Glu166	−1.9893	−1.0839	−0.2428	−0.6626
Met165	−1.0111	−1.0088	−0.0023	0
Met49	−0.8614	−0.8246	−0.0368	0
His41	−0.8522	−0.8308	−0.0214	0
Asn142	−0.8434	−0.7487	−0.0947	0
His163	−0.7228	0.0374	0	−0.7601
Gln189	−0.5892	−0.4925	−0.0967	0
Phe140	−0.4199	−0.3856	−0.0342	0
Leu167	−0.4046	−0.4046	0	0
His164	−0.3943	−0.3943	0	0

^aThe sum of steric components is the total of the weighted sum of the first three terms of the scoring function for a residue.

^bThe sum of hydrophobic components is the sum of all weighted hydrophobic(d_{ij}) terms for a residue.

^cThe sum of hydrogen-bonding components is the sum of all weighted hbonding(d_{ij}) terms for a residue; the three sums amount to the energy contribution.

DrugBank dataset and CAS COVID-19 antiviral candidate compounds dataset

The DrugBank dataset (<https://www.drugbank.ca/releases/latest>) with 1814 FDA-approved drugs was downloaded and filtered to eliminate metals or mixtures of isotopes. Moreover, CAS COVID-19 antiviral candidate compounds dataset with nearly 50 000 chemical substances was download via <https://www.cas.org/covid-19-antiviral-compounds-dataset>. VEGA [30] is applied to prepare the small molecules by adding the polar hydrogens, Vina force field and Gasteiger charges. To determine whether the tertiary (3°) amide of the small molecule should be protonated, PROPKA (version 3.1) [31] was utilized to predict the corresponding pKa values. With such values, our program-MCCS [26] is able to donorize the nitrogen atoms whose computed pKa value is greater than or equal to the given pH (7.4 by default). Finally, the torsions (branches) were also defined by VEGA, and the file format was transformed into PDBQT. The PDBQT files of protein and ligand and the pKa file of the ligand form the input of our method.

Virtual screening by MCCS

Starting with the code base of the current stable version 2.2.3 of idock [29] that adopts the exact scoring function of AutoDock Vina [28], we developed an even more efficient variant integrating the ability to calculate the residue contributions of the binding energy, named jdock [26]. MCCS is open source under Apache License 2.0 and is freely available on GitHub at <https://github.com/stcmz/jdock/> and <https://github.com/stcmz/mccsx>. MCCS was then applied to carry out the virtual screening using the crystal structure of 3CL^{Pro} in SARS-CoV-2 against the DrugBank dataset and the CAS COVID-19 antiviral candidate compounds dataset.

Virus-associated disease-specific chemogenomics knowledgebase (Virus-CKB)

On the basis of our established domain specific chemogenomics databases [32–35] and our novel computational techniques [32, 36–39], we constructed and reported a novel virus-associated disease-specific chemogenomics knowledgebase (Virus-CKB, <https://www.cbligand.org/g/virus-ckb>) [27] and applied our computational systems pharmacology-target mapping (CSP-Target Mapping) to rapidly identify the FDA-approved drugs

for repurposing into new indications by fast progress into clinical trials to meet the urgent demand due to the COVID-19 outbreak. Virus-CKB, a one-stop computing platform describes the chemical molecules, genes, proteins and signaling pathways involved in the regulation of virus-associated diseases. To date, the Virus-CKB archived 65 antiviral drugs in the market, 107 virus-related proteins or enzymes with 189 available 3D crystal or cryo-EM structures [40–42], and ~2609 chemical agents reported for these target proteins and enzymes. In addition, the Virus-CKB is implemented with our developed machine-learning computational algorithms and computing tools for the prediction of the important protein targets, and the output data analysis and visualization, including HTDocking [32, 36–38], TargetHunter [32, 36–39], BBB predictor [32, 37, 38], NGL viewer [43], Spider Plot [32, 36, 37], etc.

Results and Discussion

Workflow of MCCS protocol

We here described the general procedure of MCCS protocol as below: (1) the first step of MCCS protocol is to prepare the input files (PDBQTs) of both receptor and ligand, including the ligand protonation with PROPKA [31], residues repartition of the receptor by Chimera [44] and adding force fields and charges to receptor and ligand by VEGA [30]; (2) the second step is to calculate the residue energy contribution by our revised docking algorithm named 'jdock', which shared the same scoring function with AutoDock Vina [28] or idock [29]; (3) sequentially, a part of or a full-length protein sequence-based vector embedded with individual residue energy contribution is constructed to represent the binding recognition feature between a receptor and its ligand, name the energy recognition vector; (4) finally, the energy contribution vectors are explored for extensive uses in recognition-pattern generation, protein similarity comparison and clustering, and virtual screening. All these components have been integrated into MCCS with ready-to-use computer scripts developed in-house.

Residue energy contribution

After obtaining the input files, MCCS is used to calculate the energy contribution of each residue, which can help us to understand the role of binding residues for the recognition of ligand(s). With the aggregation accomplished, a list of scores is fetched.

Table 1 is the example of outputs of the 3CL^{Pro} in the SARS-CoV complexed SID-24808289 (N-(benzo [1,2,3] triazol-1-yl)-N-(benzyl)acetamido)phenyl)carboxamides, inhibitor) (PDB: 4MDS, Resolution: 1.598 Å) [45].

The detailed interactions between 3CL^{Pro} in SARS-CoV and SID-24808289 were shown in Figure 1. The total binding energy of the crystallized small molecule-SID-24808289 in 3CL^{Pro} was −11.7914 kcal/mol, which was calculated from the sum of intra-ligand free energy (−0.0088 kcal/mol) and inter-ligand free energy (−11.7826 kcal/mol). Here, the inter-ligand free energy is the total energy of interacted atom pairs between the small molecule (SID-24808289) and the receptor (3CL^{Pro}), which can be computed and further divided into the energy contribution of each residue. Moreover, each residue energy contribution can be further decomposed into (i) the ‘sum of steric components’ that included gauss1, gauss2 and repulsion, (ii) the ‘sum of hydrophobic components’ and (iii) the ‘sum of hydrogen-bonding components.’ Taking Glu166 in 3CL^{Pro} (PDB: 4MDS) as an example (Table 1), the total energy contribution of Glu166 to the complex of SID-24808289-3CL^{Pro} was −1.9893 kcal/mol, which can be decomposed into (i) −1.0839 kcal/mol from the ‘sum of steric components,’ (ii) −0.2428 kcal/mol from the ‘sum of hydrophobic components’ and (iii) −0.6626 kcal/mol from the ‘sum of hydrogen-bonding components.’ Particularly, we noted that Glu166 and His163 contributed significantly to the recognition of ligand SID-24808289 through hydrogen-bonding interaction (Table 1), as shown in Figure 1.

Energy contribution vectors and recognition pattern in the ligand-binding pocket of 3CL^{Pro} in SARS-CoV

Then, a protein sequence-based vector embedded with individual residue energy contribution was constructed to represent the recognition feature between a receptor and its ligand, and the most important recognition feature was named as the recognition pattern.

Using our protocol, six representative co-crystal structures of 3CL^{Pro} in SARS-CoV complexed with different ligands were selected to calculate the residue energy contribution, including 3SN8 [46], 1WOF [47], 2AMD [47], 2OP9 [48], 3V3M [49] and 4MDS [45]. For each individual complex, the total energy contribution of 73 residues within 8 Å around the co-crystal ligand was used to construct a vector named energy contribution vector (Figure 2).

As shown in Figure 2, the residue rows were sorted ascendingly according to their average contribution and the protein columns represent energy contribution vectors of each individual complex. The figure consists of 73 residues within 8 Å around the co-crystal ligand. First, our results showed that Glu166 (Figure 2) has the greatest energy contribution to the recognition of ligands with an average energy contribution of −1.5442 kcal/mol. With the insight of the residue energy contribution obtained from the analyses of these six complexes, we found that one of the key contributions of Glu166 was hydrogen-bonding interaction (Figure S1a), which was supported by the detailed interaction shown in Figure 3. Additionally, we found that residues including Gly143, Ser144, His163 and Gln189 also contributed to the recognition of ligands through hydrogen-bonding (Figure S1a). On the other hand, His41, Met49, Met165 and Leu167 contributed to the binding of ligands via hydrophobic interactions, as shown in Figure 3 and Figure S1b. Interestingly, our results showed that Cys145 contributed to the binding

by a covalent bond (red color in Figure 2, positive value) and hydrophobic interactions (blue color in Figure 2, negative value).

The energy contribution vectors of proteins could be easily compared and used to cluster similar ligands or proteins. The dendrogram on the top of the grids demonstrated the clustering of similar columns using Pearson's distance. As shown in Figure 2, we found that ligands with large similarity (or binding interactions) were clustered together, indicating our approach is reasonable for ligands classification or clustering. For example, we observed that the score vector of 1WOF was similar to that of 2AMD and these two proteins were clustered together, supported by the correlation between similarities in their ligands and interactions (Figure 3).

Our program generated nine different energy contribution vectors in total, including (1) Gauss, (2) Gauss1, (3) Gauss2, (4) hydrogen-bonding, (5) hydrophobic, (6) non-steric (hydrogen-bonding+hydrophobic), (7) repulsion, (8) steric (Gauss1 + Gauss2 + repulsion) and (9) total energy contribution, as shown in Figure S2. By analyzing these vectors of 3CL^{Pro} in SARS-CoV, we found that the non-steric recognition vector may represent the most important feature (named as recognition pattern) of 3CL^{Pro} in SARS-CoV as shown in Figure S3, which included Glu166 (hydrogen bond), Met165 (hydrophobic interaction), Met49 (hydrophobic interaction), etc. They were involved in the ligand-binding pocket in all co-crystal structures with significant contributions to the binding of small molecules. The recognition pattern of 3CL^{Pro} in SARS-CoV has taken the contribution of key residues into consideration that will benefit the accuracy of virtual screening, as the traditional docking algorithms are based on docking scores and neglects the importance of key residues.

Repurposing FDA-approved drugs for COVID-19 by recognition pattern-based computing

Using the same method, we first generated the non-steric recognition pattern (including both hydrogen-bonding and hydrophobic components) of 3CL^{Pro} in SARS-CoV-2 based on its co-crystal structure (PDB: 6LU7, inhibitor N3) [18]. Then the structure of 3CL^{Pro} in SARS-CoV-2 was used to perform a virtual screening against the prepared DrugBank library with 1814 FDA-approved drugs. Finally, the recognition patterns of each drug were used to compare with that of N3 (inhibitor in co-crystal structure), and the pattern similarity between drugs and N3 was used to select the potential hits.

Our results in Table 2 shows 10 FDA-approved drug candidates may bind to 3CL^{Pro} with therapeutic potential for COVID-19. Table S1 shows the ranking and pattern similarity of the top 100 drug candidates. For comparison, Table S2 shows the results of 10 drug candidates with the lowest pattern similarity when compared to the N3. From Table 2, we found that four anti-HIV/antiviral drugs (lopinavir, tenofovir disoproxil, fosamprenavir and ganciclovir), two antiflu drugs (peramivir and zanamivir) and one anti-HCV drug (sofosbuvir) were predicted to bind to 3CL^{Pro} in SARS-CoV-2, which could be the possible treatments for COVID-19. These drugs shared a high pattern similarity with a reported N3 inhibitor in the co-crystal complex, especially in lopinavir which shared up to 89.7% pattern similarity with N3. The comparison of detailed interactions between lopinavir and N3 in SARS-CoV-2 was shown in Figure 4. Our results showed that these two compounds shared very similar non-steric interactions (hydrogen-bonding and hydrophobic interactions), indicating

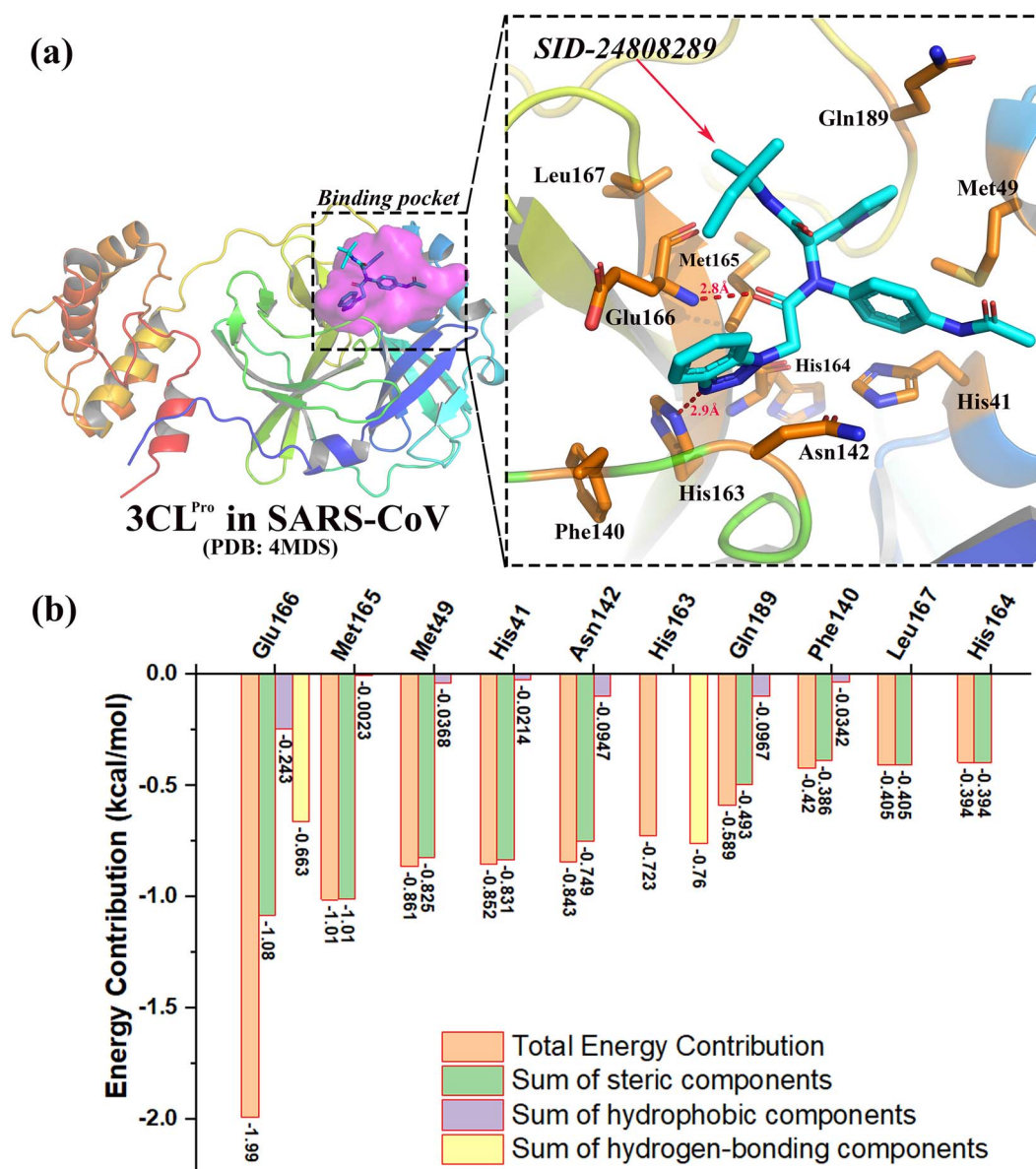


Figure 1. Detailed interactions and top 10 residue energy contributions of 3CL^{Pro}-SID-24808289 (PDB: 4MDS, SARS-CoV). (A) The detailed interactions between 3CL^{Pro} in SARS-CoV and SID-24808289. The binding pocket in 3CL^{Pro} is highlighted in purple surface on the left side. Top 10 residues with higher energy contributions are highlighted in stick on the right side. (B) The energy contribution of top 10 key residues involved in the binding pockets of 3CL^{Pro}.

that lopinavir may bind to 3CL^{Pro} in SARS-CoV-2 with therapeutic potential for the treatment of COVID-19, which is consistent with the current clinical trial of lopinavir/ritonavir for COVID-19.

In addition, recent studies [50, 51] showed that type II diabetes patients with COVID-19 develop a more severe condition compared to those without diabetes. From Table 2, we also predicted three antidiabetic drugs (acarbose, glyburide and tolazamide) with the potential to treat COVID-19 coexisting with type II diabetes [52]. Our predictions are consistent with recent work on COVID-19. For example, Wang et al. [53] suggested the roles of 21 drugs included acarbose in inflammatory response prevention in patients with COVID-19 for the first time. In addition, Paniri et al. [54] proposed that glyburide might be a useful drug to combat SARS-CoV-

2 by blocking the wide spectrum of molecules related to inflammatory cascade. Certainly, these *in silico* predictions will require the *in vitro* target validation experiments in the future.

Repurposing CAS COVID-19 antiviral candidate compounds dataset for COVID-19 by recognition pattern-based computing

MCCS was also used to predict the potential candidates from CAS COVID-19 antiviral candidate compounds dataset (<https://www.cas.org/covid-19-antiviral-compounds-dataset>). Among 50 000 compounds, 44 665 small molecules were successfully docked into 3CL^{Pro}. Table 3 shows top 10 antiviral

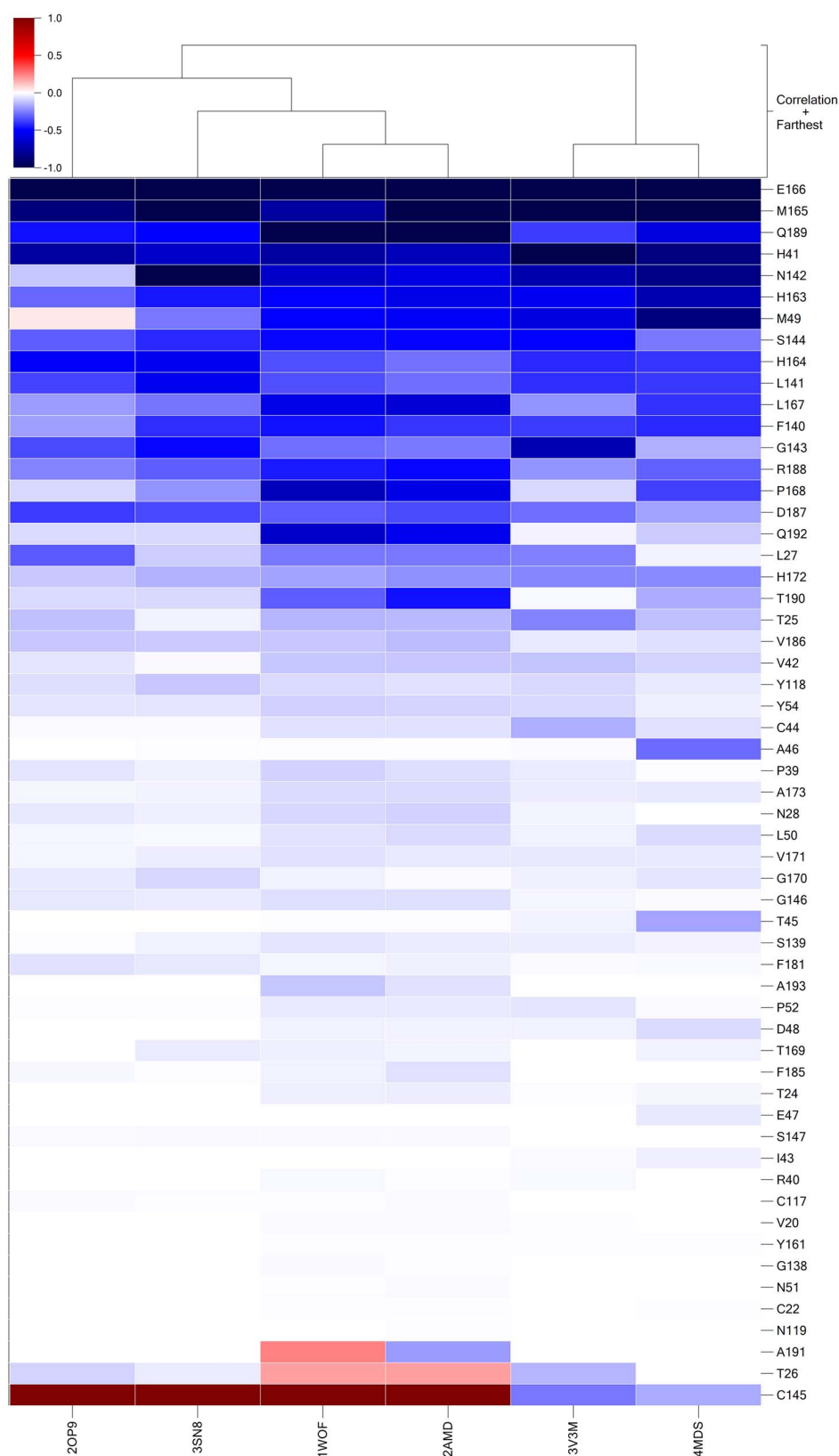


Figure 2. Energy contribution vector (using total energy contribution) in the ligand-binding pocket of 3CL^{Pro} in SARS-CoV. The dark blue color in the energy contribution vectors represented that the energy contribution of residue was negative value (≤ -1 kcal/mol), while the dark red color represented that the energy contribution of residue was positive value (≥ 1 kcal/mol). The residues in the energy contribution vectors were sorted by the average residue energy contribution ascendingly.

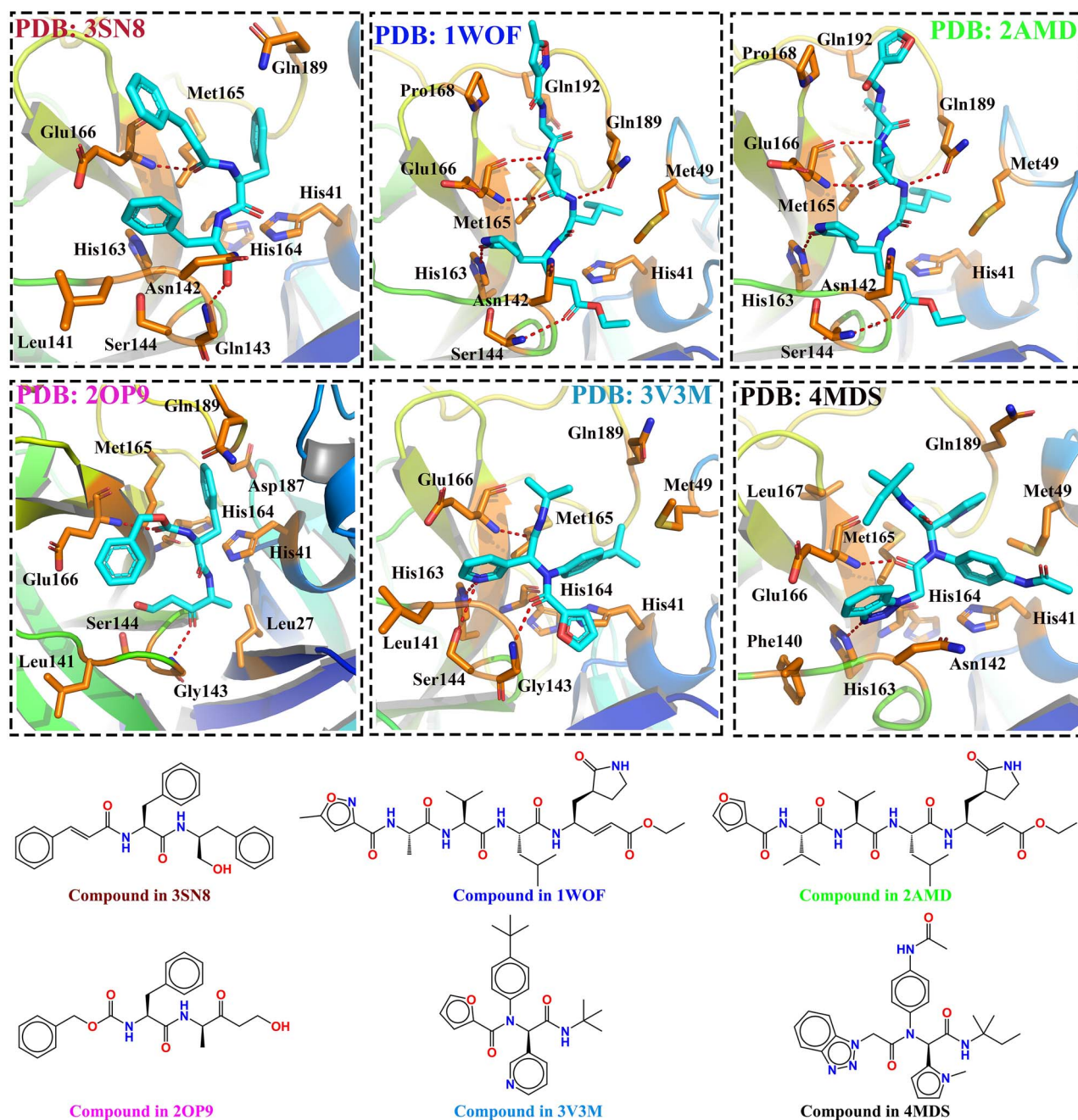
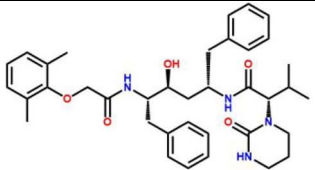
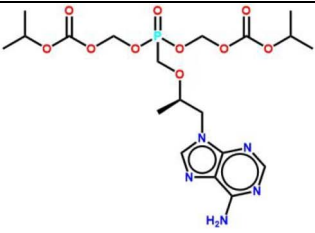
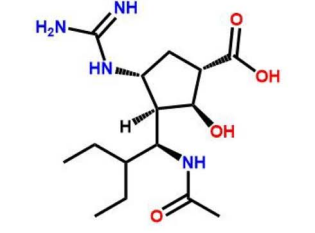
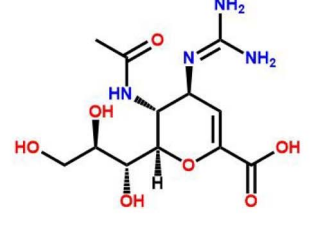
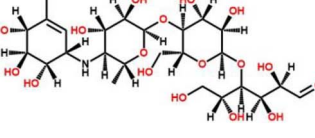
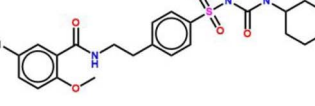
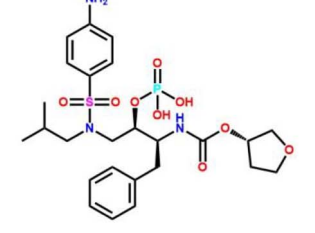


Figure 3. The detailed interactions between SARS-CoV and ligands. The hydrogen-bonding was highlighted in red. The key residues were highlighted in sticks. The structures of small molecules were shown in the bottom.

candidates may bind to 3CL^{Pro} with therapeutic potential for COVID-19. These drugs also shared a high pattern similarity with a reported N3 inhibitor in the co-crystal complex, especially the top compound (2,7,10,12-Tetraazapentadecanoic acid, 4-hydroxy-14-methyl-12-[[2-(1-methylethyl)-4-thiazolyl]methyl]-8,11-dioxo-3,6-bis(phenylmethyl)-, 5-thiazolylmethyl ester, (3S,4S,6S)-) which shared up to 97.8% pattern similarity with N3. The planning experiments will be carried out for further validations.

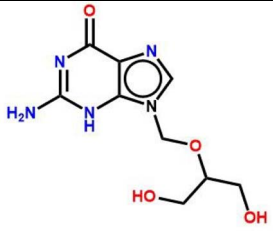

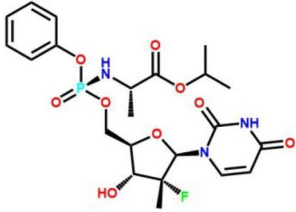
Moreover, we applied our method to explore the details of other reported SARS-CoV-2 inhibitors, including ebiselen and tideglusib from the work of Jin et al. [18] (Nature volume 582, pages289–293(2020)). Based on the detailed docking results and residue energy contribution from Figure S4, we found that several key residues in 3CL^{Pro} in SARS-CoV-2 contributed to the binding of these two ligands, including Cys145, His163, Leu141, Met49, Phe140, Asn142, His164, His41, Met165, Gln189 and Glu166. Importantly, we found that their inhibitory activities

Table 2. 10 FDA-approved drugs with therapeutic potential for COVID-19

ID	Name	Structure	Pattern Similarity	Indications	Target
1	lopinavir		89.7%	HIV	Human immunodeficiency virus type 1 protease
2	tenofovir disoproxil		88.2%	HIV and antiviral	Human immunodeficiency virus 1 protease
3	peramivir		87.6%	Influenza A/B	Influenza A virus, Influenza B virus
4	zanamivir		87.5%	Influenza A/B	Influenza A virus, Influenza B virus
5	acarbose		87.0%	Type 2 diabetes	Maltase-glucoamylase
6	glyburide		86.9%	Type 2 diabetes	Sulfonylurea receptor 1
7	fosamprenavir		86.6%	HIV	Human immunodeficiency virus type 1 protease

(Continued)

Table 2. Continued

8	ganciclovir		85.3%	Antiviral	DNA polymerase catalytic subunit
9	tolazamide		85.2%	Type 2 diabetes	Sulfonylurea receptor 1
10	sofosbuvir		84.9%	Hepatitis C virus	RNA-dependent RNA-polymerase

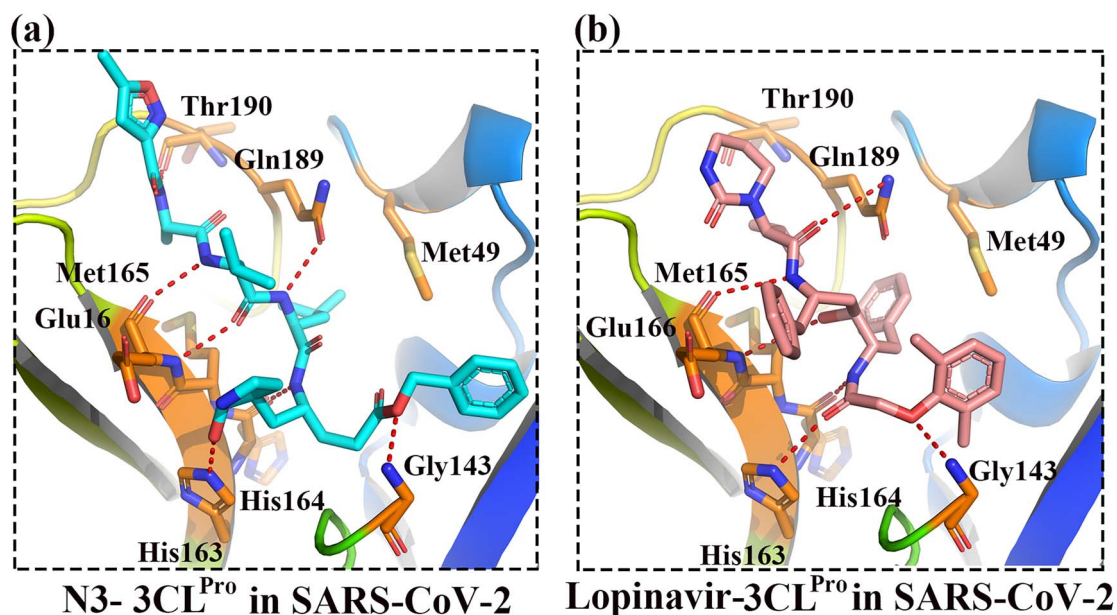


Figure 4. The comparisons between N3 (co-crystal inhibitor) and Lopinavir in SARS-CoV-2. The hydrogen-bonding was highlighted in red. The key residues were highlighted in sticks.

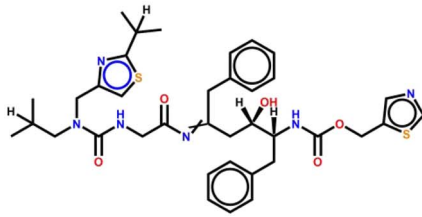
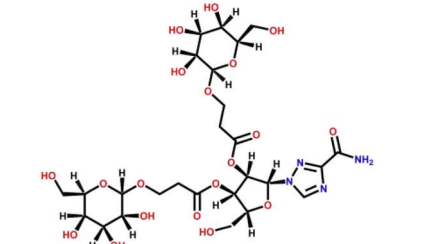
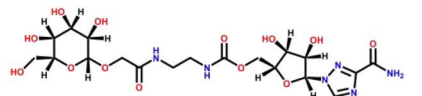
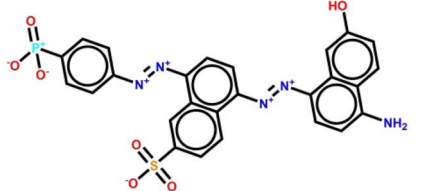
against COVID-19 may mainly attribute to a potential covalent bond formation with the thiol group of the Cys145, as shown in Figure S4a and S4b. Our results are consistent with the finding from Jin's work [18].

Virus-CKB to accelerate drug combinational therapy for COVID-19 treatment

Recently, COVID-19 patients who met the criteria for hospital discharge or discontinuation of quarantine show positive

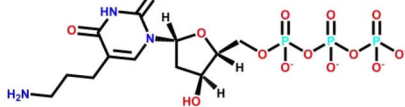
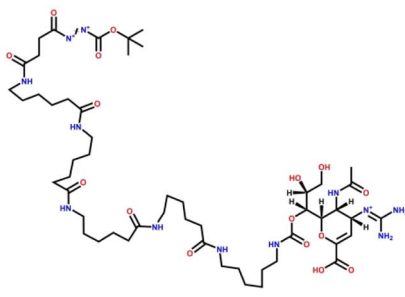
reverse transcriptase polymerase chain reaction test results even after 5 to 13 days after recovery. This suggests that at least a proportion of recovered patients may still be virus carriers [55]. In addition, co-existing diseases such as diabetes, hypertension and cardiovascular disease are found in about one-third to one-half of reported COVID-19 patients and tend to worsen the patients' prognosis [56]. These findings indicate that COVID-19 is a complex disease involving simultaneous production of signals from a multitude of transduction pathways. Therefore, a

Table 3. Top 10 CAS antiviral candidate compounds with therapeutic potential for COVID-19

ID	SMILE	Structure	Pattern Similarity	Molecular Weight	cLogP
1	<chem>CC(C)([H])c4[s]cc(CN(CC(C)(C)[H])C(=O)NCC(=O)[N+]=C(Cc1ccc1)C[C@](O)([H])[C@](H)(NC(=O)OCc2cnc[s]2)Cc3ccccc3)n4</chem>		97.8%	720.95	5.15
2	<chem>NC(=O)C1=NN(C=N1)[C@]3([H])O[C@]([H])(CO)[C@]([H])(OC(=O)CCO[C@]2([H])O[C@]([H])(CO)[C@]([H])(O)[C@]2([H])OC(=O)CCO[C@]4([H])O[C@]([H])(CO)[C@]([H])(O)[C@]([H])(O)[C@]4(O)[H])</chem>		95.2%	712..62	-5.69
3	<chem>O[C@@]2([H])[C@@]([H])(O[C@]([H])(CO)C(=O)NCCNC(=O)CO[C@]1([H])O[C@]([H])(CO)[C@]([H])(O)[C@]([H])(O)[C@]1(O)[H])C@]2(O)[H])N3C=NC(=N3)C(N)=O</chem>		95.0%	550.48	-5.12
4	<chem>[O-][P+](=O)([O-])c5ccc(/[N+]=[N+]/c3ccc(/[N+]=[N+]/c1ccc(N)c2ccc(O)cc12)c4ccc(cc34)[S](</chem>		94.7%	574.48	0.19

(Continued)

Table 3. Continued

9	<chem>O=C1NC(=O)C(=CN1[C@@]2([H])C[C@@](O)([H])[C@]([H])(O2)COP(=O)([O-])OP([O-])(=O)OP([O-])(=O)[O-])CCCN2</chem> - deoxy-		93.1%	525.24	-4.60
10	<chem>O[C@@]([H])(CO)[C@]([H])(OC(=O)NCCCCCN(C(=O)CCCCNC(=O)CCCCNC(=O)CCCCNC(=O)CCCCNC(=O)CCCCNC(=O)C(CC(=O)[N+]=[N+][C(=O)OC(C)(C)[C@]1([H])OC(=C[C@]([H])([N+]=C(N)N)[C@@]1([H])NC(=O)C)C(O)=O</chem>		92.9%	1139.36	-2.32

traditional single-target drug, though it may be highly selective and potent, may not be sufficient to effectively treat and cure COVID-19. An alternative strategy is to seek simultaneous modulation at multiple nodes in the network of virus signaling pathways through either a multi-target drug or drug-drug combinations.

On the basis of our established domain specific chemogenomics databases [32, 35] and our novel computational techniques, we constructed a virus-associated disease-specific chemogenomics knowledgebase (Virus-CKB, <https://www.cbilgand.org/g/virus-ckb>) [27] and applied our computational systems pharmacology-target mapping (CSP-Target Mapping) to accelerate drug combinational therapy to meet the urgent demand due to the COVID-19 outbreak.

To first validate our Virus-CKB, we predicted potential FDA-approved drugs that may bind to 3CL^{pro}. As shown in Figure 5, our results showed that eltrombopag (for thrombocytopenia), anidulafungin (for fungal infections), imatinib (for cancer) and proscillaridin (anti-cardiovascular) were predicted to bind to 3CL^{pro} (Node: PR_SARS2) of SARS-CoV-2. Our findings is supported by a recent study, which eltrombopag, anidulafungin, imatinib and proscillaridin exhibited antiviral efficacy (0.1 μ M < IC₅₀ < 10 μ M) against SARS-CoV-2 [57, 58].

Then, combinations of drugs with therapeutic potential for the treatment of COVID-19 are identified by our Virus-CKB and systems pharmacology-mapping program. As shown in

Figure 6, our Virus-CKB platform reveals that one green node, representing a drug target NA_INFB (Neuraminidase, Influenza B virus), connects to an anti-flu drug oseltamivir with green solid lines, which is congruent with the fact that oseltamivir shows high biological activity at its known target NA_INFB. Moreover, bictegravir (anti-HIV drug) and paritaprevir (anti-HCV drug) are also identified through Virus-CKB data analysis and computing, showing that these two drugs bind to a target of PR_SARS2, which is 3CL^{pro} of SARS-CoV-2, as highlighted by the yellow color node in Figure 6. Thus, a plausible combinational therapy is made by combining oseltamivir (anti-flu medication) with bictegravir (anti-HIV drug) and paritaprevir (anti-HCV drug) as they are targeting NA_INFB and PR_SARS2, respectively. Such combination will create a drug synergy in clinical treatment. As proof-of-evidence, some of the predictions are congruent with ongoing clinical trials registered at [ClinicalTrials.gov](https://clinicaltrials.gov), such as ASC09F + Oseltamivir and Ritonavir + Oseltamivir (<https://clinicaltrials.gov/ct2/results?cond=2019nCoV&term=&cntry=&state=&city=&dist>).

Conclusion

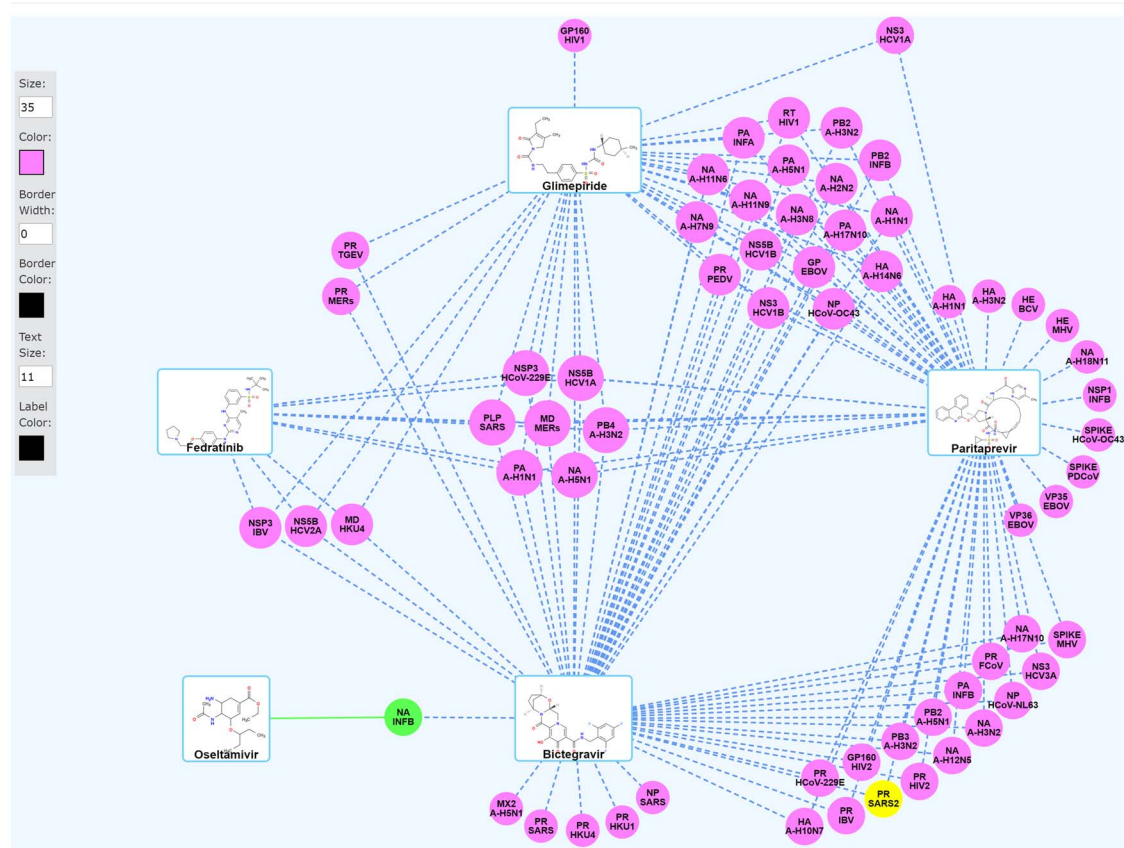
To overcome the limitation of structure-based virtual screening, we here applied our new *in silico* recognition pattern-based approach for repurposing FDA approved drugs, combining

5 Drug Combinations #119 Plot

The job was finished at 3/23/2020, 5:01:28 PM.

The number on a connection line is the average docking score in the AutoDock Vina metric.

Keyboard Guide: **Space** - Toggle label display of average docking scores **D** - Toggle depiction display



Generic Knowledgebase Computation Platform © 2018–2020 - CCGS and NIDA CDAR Centers
335 Sutherland Drive, 206 Salk Pavilion
University of Pittsburgh
Pittsburgh, PA 15261, USA

Figure 6. The predicted drug combinations for COVID-19 by CSP-Target Mapping that was implemented in our Virus-CKB. The green circles and solid lines represented the known targets and the interacted drugs, while the purple circles and dash lines represent the predicted targets and interaction, <https://www.cbligand.org/g/virus-ckb>.

Key Points

- MCCS is a scoring-function based method for characterizing the recognition pattern between protein and ligand to aid in the rational drug design.
- MCCS distinguishes itself from molecular dynamics (MD) simulation-based energy decomposition in its ability to generate the residue energy contribution and the binding recognition feature with reduced time-consumption and high accuracy.
- Recognition pattern-based method in MCCS protocol takes the importance of key residues into consideration, which helps to improve the accuracy of structure-based virtual screening.
- The use of MCCS and Virus-CKB can facilitate rapid drug development to meet the urgent demand of the COVID-19 outbreak.

Supplementary Data

Supplementary data are available at <https://academic.oup.com/bib>.

Acknowledgement

We thank Professor Zihe Rao and his group from Shanghai Institute for Advanced Immunochemical Studies (SIAIS) for the crystal structure of 3CL^{Pro} (PDB ID: 6 LU7).

Funding

Authors would like to acknowledge the funding support to Xie laboratory from the National Institutes of Health, National Institute on Drug Abuse (P30 DA035778A1).

Authors' Contributions

Z.F. and X.-Q.X. designed the project. M.C. wrote the code. Z.F. and M.C. prepared the figures and wrote the manuscript. All authors read, edited and approved the final manuscript.

Conflict of interest

The authors declare no conflict of interest.

Code and Data Availability

MCCS is open source under Apache License 2.0 and is freely available on GitHub at <https://github.com/stcmz/jdock/> and <https://github.com/stcmz/mccsx>. The example data is also available at <https://github.com/stcmz/mccs-bib-examples>.

References

- Wu JT, Leung K, Leung GM. Nowcasting and forecasting the potential domestic and international spread of the 2019-nCoV outbreak originating in Wuhan, China: a modelling study. *The Lancet* 2020;395:689–97.
- Lu R, Zhao X, Li J, et al. Genomic characterisation and epidemiology of 2019 novel coronavirus: implications for virus origins and receptor binding. *The Lancet* 2020;395:565–74.
- Zhu N, Zhang D, Wang W, et al. A novel coronavirus from patients with pneumonia in China, 2019. *N Engl J Med* 2020;382:727–33.
- Huang C, Wang Y, Li X, et al. Clinical features of patients infected with 2019 novel coronavirus in Wuhan, China. *The Lancet* 2020;395:497–506.
- Zhou P, Yang X-L, Wang X-G, et al. A pneumonia outbreak associated with a new coronavirus of probable bat origin. *Nature* 2020;579:270–3.
- Wu F, Zhao S, Yu B, et al. A new coronavirus associated with human respiratory disease in China. *Nature* 2020;579:1–8.
- Sullivan T. A tough road: cost to develop one new drug is \$2.6 billion; approval rate for drugs entering clinical development is less than 12%. *Policy & Medicine* 2019. <https://www.policymed.com/2014/12/a-tough-road-cost-to-develop-one-new-drug-is-2.6-billion-approval-rate-for-drugs-entering-clinical-de.html> (23 August 2019, date last accessed).
- Cao B, Wang Y, Wen D, et al. A trial of lopinavir-ritonavir in adults hospitalized with severe Covid-19. *N Engl J Med* 2020;382:1787–99 NEJMoa2001282.
- French Drug-Surveillance Specialist Highlights Hydroxychloroquine Risks. <https://www.wsj.com/articles/french-drug-surveillance-specialist-highlights-hydroxychloroquine-risks-11586629800> (4 May 2020, date last accessed).
- Grein J, Ohmagari N, Shin D, et al. Compassionate use of remdesivir for patients with severe Covid-19. *N Engl J Med* 2020;382:2327–36.
- Wu A, Peng Y, Huang B, et al. Genome composition and divergence of the novel coronavirus (2019-nCoV) originating in China. *Cell Host Microbe* 2020;27:325–8.
- Ralph R, Lew J, Zeng T, et al. 2019-nCoV (Wuhan virus), a novel coronavirus: human-to-human transmission, travel-related cases, and vaccine readiness. *J Infect Dev Ctries* 2020;14:3–17.
- Lai CC, Shih TP, Ko WC, et al. Severe acute respiratory syndrome coronavirus 2 (SARS-CoV-2) and coronavirus disease-2019 (COVID-19): the epidemic and the challenges. *Int J Antimicrob Agents* 2020;55:105924.
- Chowell G, Abdirizak F, Lee S, et al. Transmission characteristics of MERS and SARS in the healthcare setting: a comparative study. *BMC Med* 2015;13:210.
- Gao Y, Yan L, Huang Y, et al. Structure of the RNA-dependent RNA polymerase from COVID-19 virus. *Science* 2020;eabb7498.
- Littler DR, Gully BS, Colson RN, et al. Crystal structure of the SARS-CoV-2 non-structural protein 9, Nsp9. *iScience* 2020;23:101258 2020.2003.2028.013920.
- Lan J, Ge J, Yu J, et al. Structure of the SARS-CoV-2 spike receptor-binding domain bound to the ACE2 receptor. *Nature* 2020;581:215–20.
- Jin Z, Du X, Xu Y, et al. Structure of M(pro) from SARS-CoV-2 and discovery of its inhibitors. *Nature* 2020;582:289–93.
- Wrapp D, Wang N, Corbett KS, et al. Cryo-EM structure of the 2019-nCoV spike in the prefusion conformation. *Science* 2020;367:1260–3.
- Hoffmann M, Kleine-Weber H, Krüger N, et al. The novel coronavirus 2019 (2019-nCoV) uses the SARS-coronavirus receptor ACE2 and the cellular protease TMPRSS2 for entry into target cells. *bioRxiv* 2020.2001.2031.929042.
- Wang J. Fast identification of possible drug treatment of coronavirus disease-19 (COVID-19) through computational drug repurposing study. *J Chem Inf Model* 2020;60:3277–86.
- Liu S, Zheng Q, Wang Z. Potential covalent drugs targeting the main protease of the SARS-CoV-2 coronavirus. *Bioinformatics (Oxford, England)* 2020;36:3295–8.
- Zhou Y, Hou Y, Shen J, et al. Network-based drug repurposing for novel coronavirus 2019-nCoV/SARS-CoV-2. *Cell Discov* 2020;6:14.
- Bai Q, Tan S, Xu T, et al. MolAICal: a soft tool for 3D drug design of protein targets by artificial intelligence and classical algorithm. *Brief Bioinform* 2020;1–12. <https://academic.oup.com/bib/advance-article/doi/10.1093/bib/bba161/5890512>.
- Kong R, Yang G, Xue R, et al. COVID-19 Docking Server: a meta server for docking small molecules, peptides and antibodies against potential targets of COVID-19. *Bioinformatics* 2020;1–3.
- Xing C, Zhuang Y, Xu TH, et al. Cryo-EM structure of the human cannabinoid receptor CB2-G(i) signaling complex. *Cell* 2020;180:645–654.e613.
- Feng Z, Chen M, Liang T, et al. Virus-CKB: an integrated bioinformatics platform and analysis resource for COVID-19 research. *Brief Bioinform* 2020;1–14. <https://academic.oup.com/bib/advance-article/doi/10.1093/bib/bba155/5876604>.
- Trott O, Olson AJ. AutoDock Vina: improving the speed and accuracy of docking with a new scoring function, efficient optimization, and multithreading. *J Comput Chem* 2010;31:455–61.
- Li H, Leung K-S, Wong M-H. idock: A multithreaded virtual screening tool for flexible ligand docking. In: 2012 IEEE Symposium on Computational Intelligence in Bioinformatics and Computational Biology (CIBCB). San Diego, CA, USA: IEEE, 2012, 77–84.
- Pedretti A, Villa L, Vistoli G. VEGA—an open platform to develop chemo-bio-informatics applications, using plug-in architecture and script programming. *J Comput Aided Mol Des* 2004;18:167–73.
- Olsson MH, Søndergaard CR, Rostkowski M, et al. PROPKA3: consistent treatment of internal and surface residues

- in empirical p K a predictions. *J Chem Theory Comput* 2011;7:525–37.
32. Chen M, Jing Y, Wang L, et al. DAKB-GPCRs: an integrated computational platform for drug abuse related GPCRs. *J Chem Inf Model* 2019;59:1283–9.
 33. Xu X, Ma S, Feng Z, et al. Chemogenomics knowledge-base and systems pharmacology for hallucinogen target identification-salvinorin A as a case study. *J Mol Graph Model* 2016;70:284–95.
 34. Zhang H, Ma S, Feng Z, et al. Cardiovascular disease chemogenomics knowledgebase-guided target identification and drug synergy mechanism study of an herbal formula. *Sci Rep* 2016;6:33963.
 35. Zhang Y, Wang L, Feng Z, et al. StemCellCKB: an integrated stem cell-specific chemogenomics knowledgeBase for target identification and systems-pharmacology research. *J Chem Inf Model* 2016;56:1995–2004.
 36. Chen Y, Feng Z, Shen M, et al. Insight into Ginkgo biloba L. extract on the improved spatial learning and memory by chemogenomics knowledgebase, molecular docking, molecular dynamics simulation, and bioassay validations. *ACS omega* 2020;5:2428–39.
 37. Cheng J, Wang S, Lin W, et al. Computational systems pharmacology-target mapping for fentanyl-laced cocaine overdose. *ACS Chem Neurosci* 2019;10:3486–99.
 38. Liu H, Wang L, Lv M, et al. AlzPlatform: an Alzheimer's disease domain-specific chemogenomics knowledgebase for polypharmacology and target identification research. *J Chem Inf Model* 2014;54:1050–60.
 39. Wang L, Ma C, Wipf P, et al. TargetHunter: an in silico target identification tool for predicting therapeutic potential of small organic molecules based on chemogenomic database. *AAPS J* 2013;15:395–406.
 40. Burley SK, Berman HM, Bhikadiya C, et al. RCSB Protein Data Bank: biological macromolecular structures enabling research and education in fundamental biology, biomedicine, biotechnology and energy. *Nucleic Acids Res* 2019;47:D464–d474.
 41. Wang Y, Zhang S, Li F, et al. Therapeutic target database 2020: enriched resource for facilitating research and early development of targeted therapeutics. *Nucleic Acids Res* 2020;48:D1031–d1041.
 42. Li YH, Yu CY, Li XX, et al. Therapeutic target database update 2018: enriched resource for facilitating bench-to-clinic research of targeted therapeutics. *Nucleic Acids Res* 2018;46:D1121–d1127.
 43. Rose AS, Bradley AR, Valasatava Y, et al. NGL viewer: web-based molecular graphics for large complexes. *Bioinformatics (Oxford, England)* 2018;34:3755–8.
 44. Pettersen EF, Goddard TD, Huang CC, et al. UCSF chimera—a visualization system for exploratory research and analysis. *J Comput Chem* 2004;25:1605–12.
 45. Turlington M, Chun A, Tomar S, et al. Discovery of N-(benzo[1,2,3]triazol-1-yl)-N-(benzyl)acetamido(phenyl) carboxamides as severe acute respiratory syndrome coronavirus (SARS-CoV) 3CLpro inhibitors: identification of ML300 and noncovalent nanomolar inhibitors with an induced-fit binding. *Bioorg Med Chem Lett* 2013;23:6172–7.
 46. Zhu L, George S, Schmidt MF, et al. Peptide aldehyde inhibitors challenge the substrate specificity of the SARS-coronavirus main protease. *Antiviral Res* 2011;92:204–12.
 47. Yang H, Xie W, Xue X, et al. Design of wide-spectrum inhibitors targeting coronavirus main proteases. *PLoS Biol* 2005;3:e324.
 48. Goetz D, Choe Y, Hansell E, et al. Substrate specificity profiling and identification of a new class of inhibitor for the major protease of the SARS coronavirus. *Biochemistry* 2007;46:8744–52.
 49. Jacobs J, Grum-Tokars V, Zhou Y, et al. Discovery, synthesis, and structure-based optimization of a series of N-(tert-butyl)-2-(N-arylamido)-2-(pyridin-3-yl) acetamides (ML188) as potent noncovalent small molecule inhibitors of the severe acute respiratory syndrome coronavirus (SARS-CoV) 3CL protease. *J Med Chem* 2013;56:534–6.
 50. Xu Z, Wang Z, Wang S, et al. The impact of type 2 diabetes and its management on the prognosis of patients with severe COVID-19. *J Diabetes* 2020;1–10. <https://onlinelibrary.wiley.com/doi/epdf/10.1111/1753-0407.13084>.
 51. Guo W, Li M, Dong Y, et al. Diabetes is a risk factor for the progression and prognosis of COVID-19. *Diabetes Metab Res Rev* 2020;e3319. doi: [10.1002/dmrr.3319](https://doi.org/10.1002/dmrr.3319). Epub ahead of print. PMID: 32233013; PMCID: PMC7228407.
 52. Wang D, Hu B, Hu C, et al. Clinical characteristics of 138 hospitalized patients with 2019 novel coronavirus-infected pneumonia in Wuhan, China. *JAMA* 2020;323:1061–9.
 53. Wang X, Bin B, Xu Z, et al. Network representation learning-based drug mechanism discovery and anti-inflammatory response against COVID-19. *ChemRxiv*. Preprint 2020. <https://doi.org/10.26434/chemrxiv.12531314.v2>.
 54. Paniri A, Akhavan-Niaki H. Emerging role of IL-6 and NLRP3 inflammasome as potential therapeutic targets to combat COVID-19: role of lncRNAs in cytokine storm modulation. *Life Sci* 2020;257:118114.
 55. Lan L, Xu D, Ye G, et al. Positive RT-PCR test results in patients recovered from COVID-19. *JAMA* 2020;323:1502–3.
 56. Guan WJ, Ni ZY, Hu Y, et al. Clinical characteristics of coronavirus disease 2019 in China. *N Engl J Med* 2020;382:1708–20.
 57. Jeon S, Ko M, Lee J, et al. Identification of antiviral drug candidates against SARS-CoV-2 from FDA-approved drugs. *Antimicrob Agents Chemother* 2020;64:e00819–20.
 58. Weston S, Coleman CM, Sisk JM, et al. Broad anti-coronaviral activity of FDA approved drugs against SARS-CoV-2 in vitro and SARS-CoV in vivo. *J Virol* 2020;JV1.01218–20. doi: [10.1128/JVI.01218-20](https://doi.org/10.1128/JVI.01218-20). Epub ahead of print. PMID: 32817221.